Deriving Effective Mesoscale Potentials from Atomistic Simulations

DIRK REITH, MATHIAS PÜTZ, FLORIAN MÜLLER-PLATHE*
Max-Planck-Institut für Polymerforschung, D-55128 Mainz, Germany

Received 22 November 2002; Accepted 11 April 2003

Abstract: We demonstrate how an iterative method for potential inversion from distribution functions developed for simple liquid systems can be generalized to polymer systems. It uses the differences in the potentials of mean force between the distribution functions generated from a guessed potential and the true distribution functions to improve the effective potential successively. The optimization algorithm is very powerful: convergence is reached for every trial function in few iterations. As an extensive test case we coarse-grained an atomistic all-atom model of polyisoprene (PI) using a 13:1 reduction of the degrees of freedom. This procedure was performed for PI solutions as well as for a PI melt. Comparisons of the obtained force fields are drawn. They prove that it is not possible to use a single force field for different concentration regimes.

 J Comput Chem 24: 1624–1636, 2003

Key words: polymers; mesoscopic potential; automatic parameterization

Introduction

In polymer theory, there is still a strong focus on developing a qualitative understanding of many fundamental problems, like polymer dynamics in different environments, crystallization, or the thermodynamics of complex polymer systems. Most computational studies of specific polymers are based on atomistic models and tools developed to address specific local aspects of polymer behavior. While these methods are quite useful to gain qualitative insight, quantitative predictions of the behavior of entire chains are very hard to obtain from them.

Although computational power increases 10-fold every 5 years,[1] the huge number of degrees of freedom limits brute force approaches when it comes to investigating phenomena at meso- and macroscopic length scales. One way to circumvent this problem is to reduce the degrees of freedom by coarsening the models and keeping only those degrees of freedom that are deemed relevant for the particular range of interest. Simple models for the study of meso- and macroscale phenomena in polymers have been used extensively.[2,3] Because of their generic nature, however, most of them do not distinguish between chemically different polymers. The present contribution describes a method for systematically generating mesoscale models from atomistic models. The mesoscale or coarse-grained (CG) models contain enough information to retain the chemical identity of the parent polymer. Thus, they are able to describe specific polymeric systems.

The idea of coarse graining is not new.[4–8] To highlight a few approaches, Murat and Kremer[9] mapped bead-spring type polymer chains in a melt to a soft-core liquid with fluctuating ellipsoidal particles modeled by an anisotropic Gaussian potential. A similar way to coarsen polymer chains in dilute to semidilute solutions was recently found by Louis et al.[10,11] Closest to our approach, Tschöp and successors[12,13] and Akkermans et al.[14] did systematic studies of polymer melt coarse graining. However, none of these derived an automatic optimization scheme to conserve the chemical nature of the underlying atomistic model in a standardized way as we do.

Because of the similarity of the coarsened polymer model to simple liquids one might ask if the well-developed arsenal for simple liquids can solve the inversion problem of going from measured quantities like pair correlation functions to effective model potentials. The polymer connectivity and the fact that we deal with coarsened "super-atoms" complicates the matter significantly. Nonetheless, the self-consistent polymer reference interaction site model (PRISM) theory, developed by Schweizer and Curro,[15] combined with Monte-Carlo methods, was shown to be able to qualitatively predict both short- and long-range structures of polymer chains in melts.[16,17] So far, a route to apply PRISM theory to obtain coarse-grained potentials has not been established. Reverse Monte-Carlo (RMC) techniques[18–20] simulate a particle system to produce the correct radial distribution function (RDF)

Correspondence to: F. Müller-Plathe; e-mail: f.mueller-plathe@iu-bremen.de

*Permanent address: International University Bremen, P.O. Box 750561, D-28725 Bremen, Germany

without the explicit need for a potential. The lack of a potential, though, limits the usefulness of the approach. As explained in ref. 21, RMC methods are useful for obtaining higher order correlation functions from the knowledge of the pair distribution functions, without knowing the underlying forces. Attempts similar in spirit to RMC have also been developed by Lyubartsev and Laaksonen[22] and were later applied to DNA studies.[23]

From a practical point of view, it is desirable to establish a standard framework for coarse-graining of polymer systems, that is, a formalism that allows one to calculate a broad range of properties with a minimum amount of manual interference. We developed an automatic and iterative way to determine effective interactions that properly match a set of quantities calculated from a higher detailed reference simulation model (i.e., atomistic). While in principle one could also use experimental reference data (as has been done in the related problem of atomistic force field optimization[24]), the structural distributions needed here are difficult or impossible to measure with sufficient accuracy.

To map atomistic to mesoscopic models, one groups several atoms together into "super-atoms." On this coarsened length scale, effective potentials are sought in an optimization procedure that reproduces the structural distributions between the super-atoms, as obtained from a simulation of the atomistic model. Reith et al.[25] successfully applied a simplex algorithm to such an optimization. However, slow convergence of the analytical potentials and the manual process of selecting a good functional form of the potential are drawbacks of this method. The new approach presented here removes some of the ambiguity by using tabulated numerical potentials instead. The method is called iterative Boltzmann inversion.

It shall be introduced as follows: In the next section, we derive our inversion method for polymer models. Then, we test the convergence of the inversion scheme on a simple Lennard-Jones (LJ) liquid and discuss ways of improving the convergence rate. Then, we show how the method is applied to obtain CG potentials from atomistic simulation data for the example of polyisoprene. The resulting CG model reproduces a chosen set of structural details of the atomistic system to very high accuracy.

Iterative Boltzmann Inversion

The general problem of creating a realistic model consists of writing down a Hamiltonian that can then be parametrized to reproduce empirical information about a system as well as possible. To define the Hamiltonian, one needs to choose a set of particles and interactions between them. The choice of these variables (in our context CG super-atoms, how many of them, their relation to the underlying real atoms) can hardly be automated and a good choice will probably always depend on one's physical intuition. Hence, although important, we pay little attention to this part of the problem in this work. The interactions between the particles have most commonly been chosen to be analytic functions with a few adjustable parameters. Observables can usually be expressed as functionals of correlation functions between the various degrees of freedom. It has been argued that if all interactions with potentials $V^{(n)}(r_1, \ldots, r_N)$ (x_i labeling the degrees of freedom) in an atomistic system consist of n-body and lower terms, then the system is completely determined by the knowledge of all correlation functions $g^{(n)}(x_1, \ldots, x_N)$ of nth order and lower (cf. ref. 26). In practice a complete determination of n-point ($n > 4$) correlation functions for $N > 2$ particles is a huge task for all but the simplest model cases and one typically has to restrict oneself to a limited subset. Even if one knew all relevant correlation functions for a statistical mechanical system, one would still have to face a high-dimensional nonlinear inversion problem to derive the set of effective potentials. Here, we limit ourselves to correlation functions that only depend on a single coordinate, like RDFs [$g(r)$], bond distance [$d(r)$], bending angle [$a(\alpha)$], and dihedral angle distributions [$b(\beta)$]. These distribution functions and variables are a convenient choice to describe the structure of polymers, because they allow a separation of intra- and intermolecular structure that is naturally motivated by the chemical connectivity of polymer chains. They enable the use of an iterative Boltzmann inversion scheme to extract effective potentials from a set of known correlation functions.

Let us illustrate the procedure with the example of deriving an effective nonbonded potential $V_0(r)$ from a given RDF $g(r)$. We first need a reasonable initial guess. It has been proposed[20] to invert RDFs for one-component simple liquid systems by taking a simple Boltzmann inverse of $g(r)$. This is, however, exact only in the limit of infinitely dilute systems, that is, with density $\rho = 0$. We use the potential of mean force

$$F(r) = -k_B T \ln g(r) \tag{1}$$

which is a free energy and not a potential energy (except for the uninteresting case of zero density). However, $F(r)$ is usually sufficient to serve as the initial guess $V_0(r)$ for an iterative procedure. (Other choices are possible as well, e.g., hard spheres.) Simulating our system with $V_0(r)$ will yield a corresponding $g_0(r)$, which is different from $g(r)$. The potential needs to be improved, which can be done by a correction term $-k_B T \ln[g_0(r)/g(r)]$. This step can be iterated:

$$V_{i+1}(r) = V_i(r) - k_B T \ln\left(\frac{g_i(r)}{g(r)}\right) \tag{2}$$

This is illustrated in Figure 1. Clearly a potential that reproduces $g(r)$ is a fixed point of the iteration. Thus, if the algorithm converges we have a valid solution. Soper[20] gives some qualitative arguments why one can expect convergence. In general, each iteration tends to over-correct the current potential, as we demonstrate for a simple LJ test case in the next section.

A generalization to more than one potential/distribution function pair is straightforward. We simply have to replace the potential $V(r)$ and distribution function $g(r)$ by the appropriate pair of functions, for example, $V_{\text{bend}}(\theta)$ and $a(\theta)$ in the case of an intramolecular bending interaction. Because in dense systems individual distributions usually depend on the full set of potentials through higher-order correlations, one cannot simply iterate for each potential separately. Although one can keep all other potentials constant while iterating a particular one, one must readjust after other potentials are changed. For practical purposes, one should start with those potentials that are least affected by changes

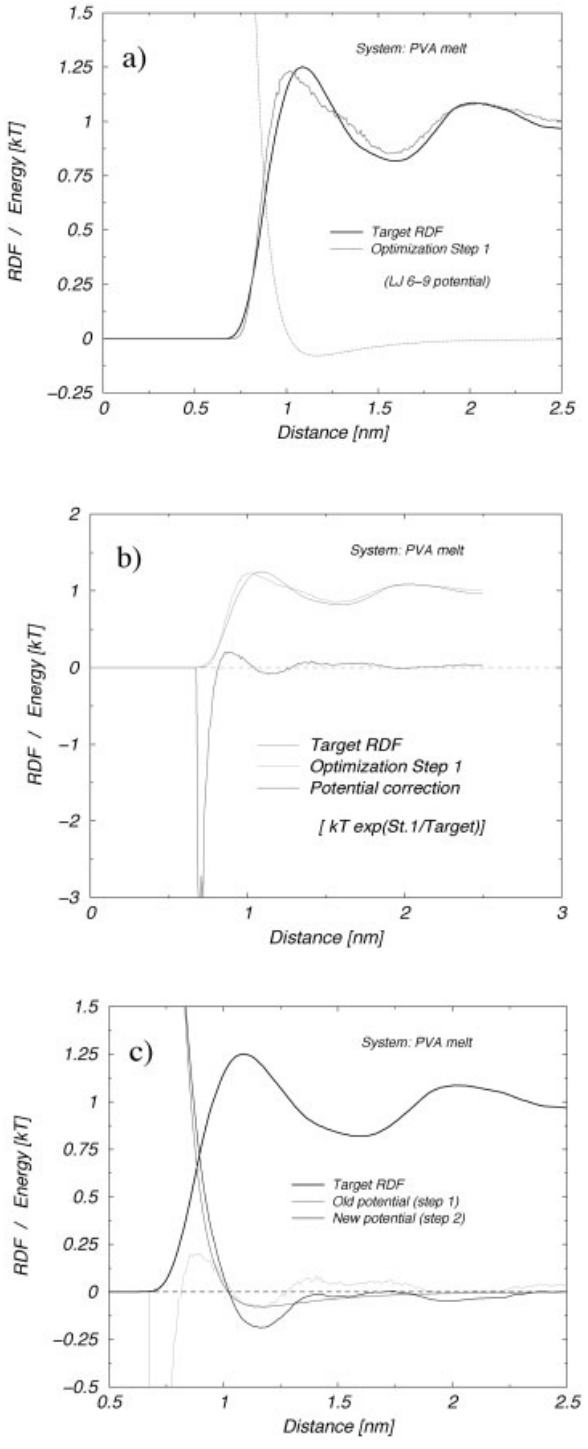

Figure 1. Illustration of the iterative procedure. (a) A test simulation (step 1) is executed with an arbitrary chosen initial potential. This results in a trial RDF for this first optimization step. (b) Taking the ratio between trial and target RDF leads via Boltzmann-inversion to a potential correction. (c) By adding the correction to the old potential, the new potential for the next iteration (step 2) is generated.

to all other ones, for example, bending potentials before nonbonded potentials. The speed of convergence can be influenced strongly by the order in which one optimizes the various potentials, and, in the case of nonbonded interactions, by limiting the range of the potentials. The latter will be demonstrated in depth in the following section. All details of implementation have been published separately,[27] in order to streamline the flow of the physical arguments.

Convergence Tests with Model Liquids

For the method to be useful, it should converge rapidly, the resulting potential should be physically sensible, and it should find the correct potentials in known test cases. An additional consideration arises from the fact that the same RDF can be reproduced to within its uncertainties by several visibly different potentials, as will be shown below. Hence, it is useful to establish criteria for selecting a specific one from a set of potentials.

Before trying polymers, we therefore tested the iteration scheme with two dense model liquids ($\rho^* = 0.85$, $T^* = 1$ in reduced units[28]): we applied firstly the purely repulsive Weeks-Chandler-Andersen (WCA) potential,[28] which equals zero for $r > 2^{1/6}\sigma$, and secondly, the LJ(6-12)-potential, with a cutoff distance of $r_{cut} = 2.5\sigma$. Both systems contained $N = 1024$ particles and were simulated in the NVT ensemble. As target function to be reproduced, we chose the RDFs corresponding to the nonbonded WCA or LJ potential, respectively. We want to emphasize the point that here we were in the comfortable but rare situation of knowing *exactly* the correct potential function(s) and, hence, the solution(s) of the inversion problem. Each system was simulated for $10^5\tau$ (τ is the LJ-time[28]) to obtain smooth RDFs, which we calculated in the range $r \in [0; 4.5\sigma]$ with $\Delta r = 0.01\sigma$.

Firstly, we tested the numerical stability of our iterative potential solver. In both cases, we used the correct potential with an extended range as input, padding it with zeros. In case of the LJ liquid, the extension reached from 2.5σ to 3σ, in the case of the WCA liquid from $\sqrt[6]{2}\,\sigma$ to 2.5σ. That is, we tested how far the algorithm moves away if started with the perfect solution. We observed that the iterations introduced nonzero values (below $\pm 0.02 k_B T$) of the potential beyond the range of the true potential, which are clearly artifacts. They could be nearly removed by smoothing both the trial RDFs and the iteratively changed trial potentials. Without smoothing, the statistical noise is too large to conserve the initial potential shape for $r > r_{cut}$. But a five-point running average was sufficient to maintain the correct shape, as shown in Figure 2. Part (a) shows the results for the WCA potential. Even after 35 iterations, the energy fluctuations at large $r > r_{cut}$ are below $0.005 k_B T$, being in the same order of magnitude as the fluctuations from an intermediate run. Similar deviations were found for the LJ liquid (Fig. 2b). The problem is that unphysical fluctuations on the scale of the mesh are not sufficiently suppressed for large r within the accuracy of our calculations. A strong positive peak in the potential at a particular mesh point countered by a negative peak in directly neighboring mesh point disturbs the resulting RDF only very weakly, especially if they occur at large r. Hence, they have a tendency to destabilize the

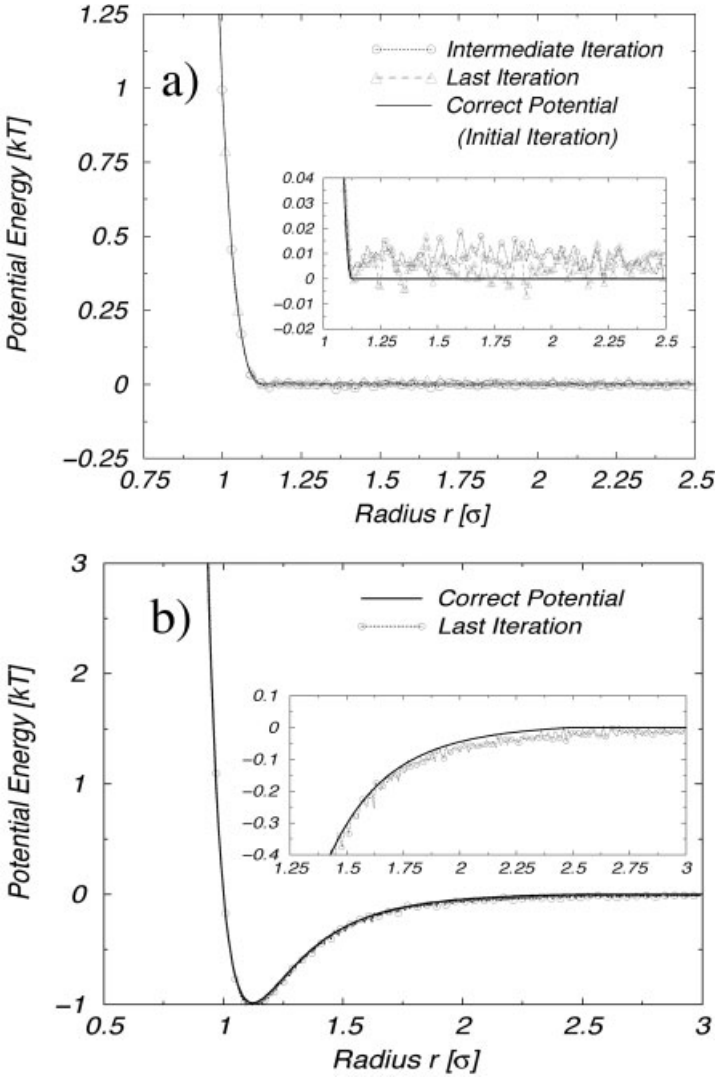

Figure 2. Stability test of iteratively optimized potential functions for a dense liquid of (a) WCA and (b) Lennard-Jones model atoms. Although being short-ranged [(a) $\approx 1.1\sigma$, (b) 2.5σ], the true potentials were chosen as initial guesses of a long-ranged artificial optimization. In each step, a five-point running average was applied to both the trial RDF and to the new potential. The potential shape remains the same during a total of 35 iteration steps; for reasons of clarity, only a few iterations are shown. It should be noted that all potentials shown here reproduced the corresponding radial distribution functions to within line thickness.

procedure and therefore have to be suppressed by additional means, that is, some convenient smoothing algorithm. This could be a problem if the RDF structure shows strong gradients. Then the smoothing algorithm has to be chosen very carefully to conserve the real physical features.

Secondly, we investigated if the correct potential is retrieved when we start the iterations from the Boltzmann-inverted function of the target RDF. These optimizations are done for various ranges of r in order to check what happens if the range does not match the range of the true potential. Starting from the Boltzmann-inverted potential, the target RDF is not matched immediately, but 3–10 iterations yield the correct shape (RDFs match within their fluctuations). This underlines the robustness of the method.

The situation is not quite as favorable for the corresponding potential functions. For the WCA system, the results are given in Figure 3. In all cases, the optimization starts from the Boltzmann-inverted potential of the target RDF. The r-ranges for the numerical potential were chosen according to the position of the minima in the target RDF: (a) 4.5σ, (b) 2.5σ, and (c) 1.6σ. We picked the minima because we expect in the valleys fewer particles that have

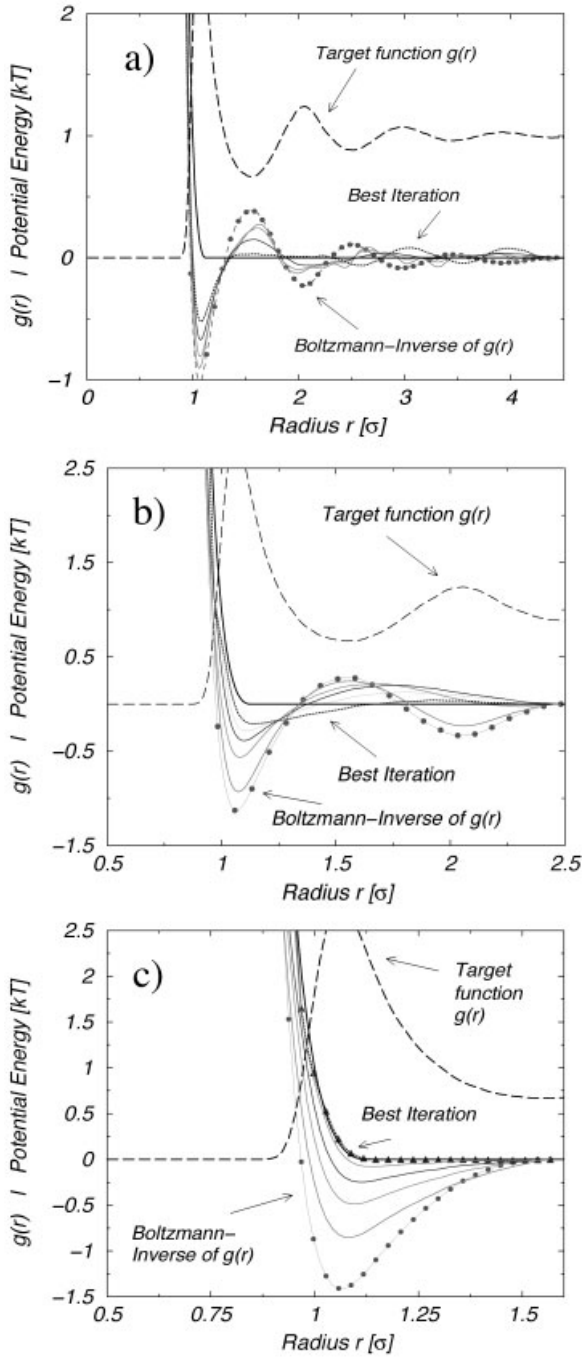

Figure 3. Potential reproduction test for a dense liquid of WCA model particles. In all cases, the iteration starts from the Boltzmann-inverted potential of the target RDF. The range of the numerical potential is (a) 4.5σ, (b) 2.5σ, (c) 1.6σ. For reasons of clarity, graphs from only some iteration steps are drawn. In every case, the target RDF can be quickly reproduced, but only for (c) the converged potential is purely repulsive.

to experience the force discontinuity when entering the range of the potential. For case (a) we executed 15 iterations until we decided that the long-ranged fluctuations were unlikely to disappear in an acceptable number of iterations, even though there was a tendency to reduce the depth of the first potential minimum ($0.5k_BT$). Case (b) was iterated for 28 steps and the result was much better: the depth of the first minimum could be significantly reduced ($0.25k_BT$) and for $r > 1.5\sigma$ the potential decayed almost to zero. However, further progress was slow so that we stopped the optimization. In the last case (c), we could reach the original potential shape within line thickness after 13 steps and it remained stable thereafter, as expected from the previous test.

For the LJ system (note: $r_{cut} = 2.5\sigma$), we tried two different ranges of optimizations (cf. Fig. 4): (a) 2.05σ, (b) 2.5σ. In case (a) we could see how robust the method was with an unfavorable cut-off: firstly, it is shorter ranged than the true one, and secondly, we cut it off at a peak value in the RDF, generating (with the initial

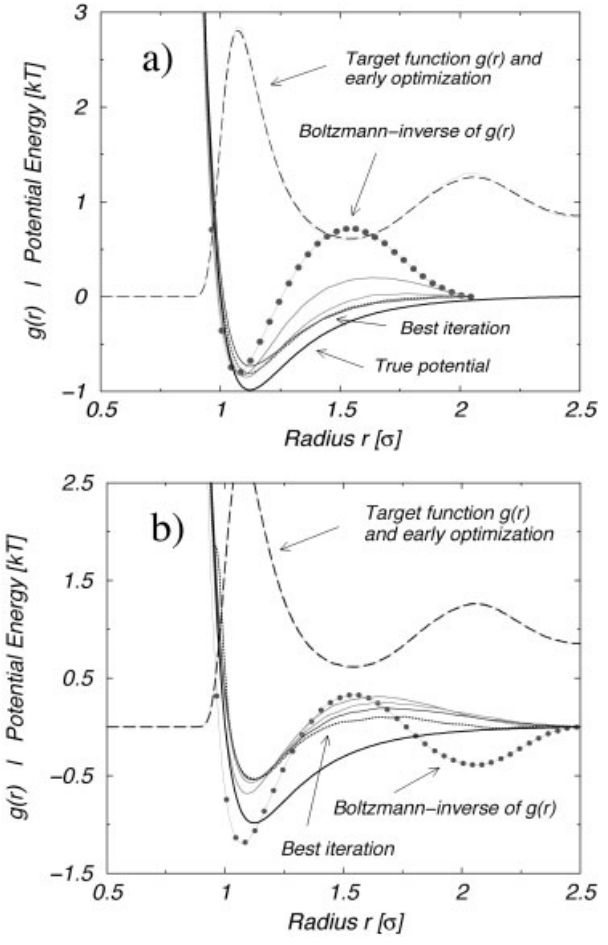

Figure 4. Potential reproduction test for a dense liquid of LJ model particles. In both cases, the optimization starts from the Boltzmann-inverted potential of the target RDF. The range of optimization is (a) 2.05σ, (b) 2.5σ. The latter equals the cut-off range of the original LJ system. For reasons of clarity, graphs from only some iteration steps are drawn. In every case, the target RDF can be quickly reproduced, however, the best iterative potentials do not exactly match the original function. By watching the slope note that the derivatives (i.e., the forces) match very well up to $r \approx 1.5\sigma$.

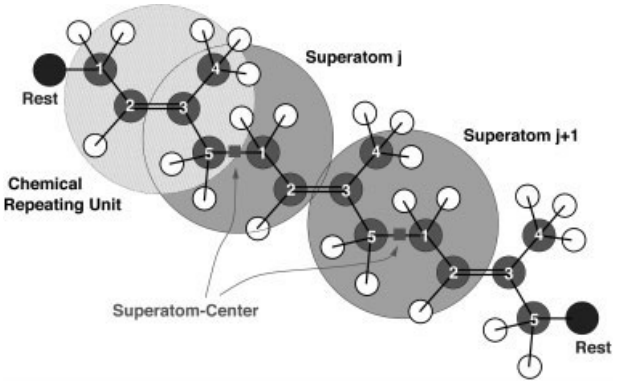

Figure 5. Illustration of the mapping of *trans*-1,4-polyisoprene from the atomistic to the mesoscopic level. Each chemical repeat unit is represented by one super-atom. As center of these super-atoms, we choose the middle of the atomistic bond between two successive chemical repeat units. This is useful because the resulting mapped chains generate well-defined peaks for the various intramolecular distributions.

Boltzmann-inverted RDF as the potential guess) the situation that particles coming into the range of the potential first experience a repulsion instead of the physically meaningful London attraction. The result was as expected: the artificial repulsive part around 1.5σ had vanished completely and the slope of the final potential almost matched the slope of the true potential, that is, the forces are very similar. In fact, this result was even better than what we obtained for the correct range in case (b). Here, the attraction at around $r \approx 2\sigma$ slowed down the convergence and the decrease of the nonphysical repulsion at around $r \approx 1.5\sigma$. Up to this distance, however, the forces were nicely matched, too. Taken together, our new iteration scheme satisfies the demands of stability and qualitative reproduction of the true potential function. However, in practice there can be many (similar) potential functions that can reproduce a given target RDF, even in the simple case of monoatomic dense liquid systems. For practical as well as for physical reasons, it makes sense to choose the shortest-range potential that reproduces the RDF, from a selection of possibilities. Alterations may be done thereafter by increasing the potential and RDF range successively in a series of optimizations until one is satisfied with the reproduction of the target RDF. Note also, that we did not yet explore the field of well-known convergence accelerators (e.g., shifting cut-off or dynamic prefactors for the correction term[20]) except for our simple working solutions.

Polyisoprene: Coarse Graining of a Realistic Model

All coarse-grained force fields depend on system properties like density, temperature, and composition. This was explicitly clarified in the section Iterative Boltzmann Inversion. Therefore, for two different concentrations, a melt and dilute solution, two force fields had to be constructed. The choice of the mapping centers was identical. Therefore, we first describe the technical details and the mapping procedure common to both systems. Subsequently, the specific optimizations will be discussed.

Technical Simulation Details

The atomistic simulations that are our starting point for the coarse graining are described in detail in ref. 29 in the case of the melt and in ref. 30 in the case of the solution. We only briefly summarize the main characteristics. The melt simulation contained 100 oligomers of length 10 monomers at a density of 890 kg/m^3. All chains were *trans*-polyisoprene (cf. Fig. 5). We applied a self-developed all-atom force-field resulting in 132 interaction sites or atoms per chain. The atomistic simulation lasted 1.1 ns at ambient conditions ($T = 300$ K, $p = 101.3$ kPa). This model describes the relaxation of local time correlation functions in agreement with NMR measurements and it reproduces the melt structure factor of polyisoprene[31] reasonably well.

The solution simulation was done with one single strand of 15 monomers dissolved in cyclohexane. We chose ambient conditions with a density of 763 kg/m^3 and a polymer concentration of weight 4.6%. The polymer force field was the same as in the melt case except that only interactions up to four neighbors were excluded. Some thermodynamic and static properties of the atomistic systems are listed in Table 1, following the nomenclature applied in ref. 30.

For the CG simulations, both MD (for the melt) and Monte Carlo (MC; for the solution) programs were used. All MD runs were performed in the *NVT* ensemble. The system consisted of an orthorhombic box with periodic boundary conditions. The Langevin equations of motion were integrated by the velocity Verlet algorithm with a time step $\Delta t = 0.01\tau$.[28] A mean temperature of

Table 1. Characteristic Properties of the Atomistic Polyisoprene (PI) Simulations.

System	N_P	N_C	c	ρ [kg/m^3]	t_{sim} [ns]	R_H [nm]	R_G [nm]	R_e^2/R_G^2
M1	100	0	100%	890.0	1.18	1.13 ± 0.07	0.76 ± 0.05	6.0
S1	1	250	4.6%	764.2	11.25	1.33 ± 0.12	1.21 ± 0.20	6.1
S3	2	500	4.6%	762.5	7.81	1.34 ± 0.10	1.23 ± 0.20	6.5

The systems labels follow the nomenclature applied in ref. 30. N_P is the number of PI oligomers (10-mers in the melt and 15-mers in solution) and N_C the number of cyclohexane molecules. c is the concentration in weight % polymer. t_{sim} is the simulated time for the systems. R_H refers to the hydrodynamic radius, R_G to the radius of gyration, and R_e to the end-to-end distance of the PI oligomer strands.

$k_BT = 1$ was maintained by the Langevin thermostat with friction constant $\Gamma = 0.5\tau^{-1}$.[32] For the MC simulations, the single chain program PRISM[17] was applied. It applies various kinds of Pivot moves to simulate a canonical ensemble. We carried out 10^5 attempted warm-up moves before a production run of 10^6 attempted MC moves was started (acceptance rate varied typically between 5 and 10%).

Mapping Procedure

The mapping to the mesoscale is sketched in Figure 5. Each chemical repeat unit is replaced by one super-atom, centered at the middle of the atomistic single bond between two successive chemical repeat units. Consequently, an atomistic N-mer is coarse grained to a $N-1$-mer, disregarding the two remainders at either end. This mapping scheme generates peaks that are well distinguishable for the various intramolecular distributions. This result follows from the nature of the chemical bonds of the backbone: every double bond is followed by three single bonds. If one chose the center of mass of the chemical monomer, the connection between successive super-atoms would be mediated by the C_5—C_1 single bond. Our choice separates two super-atoms by the C_2—C_3 double bond, which has negligible configurational freedom, and leads to sharper peaks on the mesoscale. Moreover, the chemical repeat unit centered around the double bond is flat; all carbon atoms of one monomer lie in one plane. Our studies on low molecular weight liquids showed that such conditions are unfavorable for CG procedures in which the super-atoms are represented by spheres.[33] In contrast, the C_5—C_1-centered super-atom includes three single bonds, which makes it more spherical. Resulting distributions for intramolecular degrees of freedom are shown in Figure 6, both for the melt and for the solution. For the latter, the graphs are arithmetic means of all three PI oligomer strands of the systems S1 and S3, for statistical reasons (for details and nomenclature, compare ref. 30). Histogram (a) represents the angle between three successive CG super-atoms, (b) the dihedral for four successive super-atoms. They indicate that the chains are more curved in the melts than in solution: there is a larger proportion of angles around 90°, in addition to the majority of dihedral angles being around 360°, which in our notation means that the chain is folded back onto itself (180° corresponds to the fully stretched *trans* conformation).

The distribution of distances between two adjacent super-atoms is well approximated by a Gaussian, centered at $\bar{m} = 0.469$ nm with a standard deviation of $\sigma_{\bar{m}} = 0.015$ nm (not shown here). For the bond stretching, we therefore used a simple harmonic potential. In addition to the full intramolecular RDF, we also calculated the so-called RDF-a and RDF-b. RDF-a refers to an intrachain RDF ignoring the first neighbors along the chain. RDF-b denotes the intrachain RDF excluding first and second neighbors. The difference between the full RDF and RDF-a (cf. Fig. 7) shows that the main peak (0.469 nm) originates from adjacent super-atoms. The difference between the RDF-a and RDF-b reveals that the second peak around 0.9 nm mainly comes from the second neighbors. It corresponds to the peak close to 160° in Figure 6a. The second peak around 90° in this figure gives rise to a hump at around 0.65 nm in Figure 7 that it is less pronounced. The rise of the RDF-b at very short distances and its substantial intensity

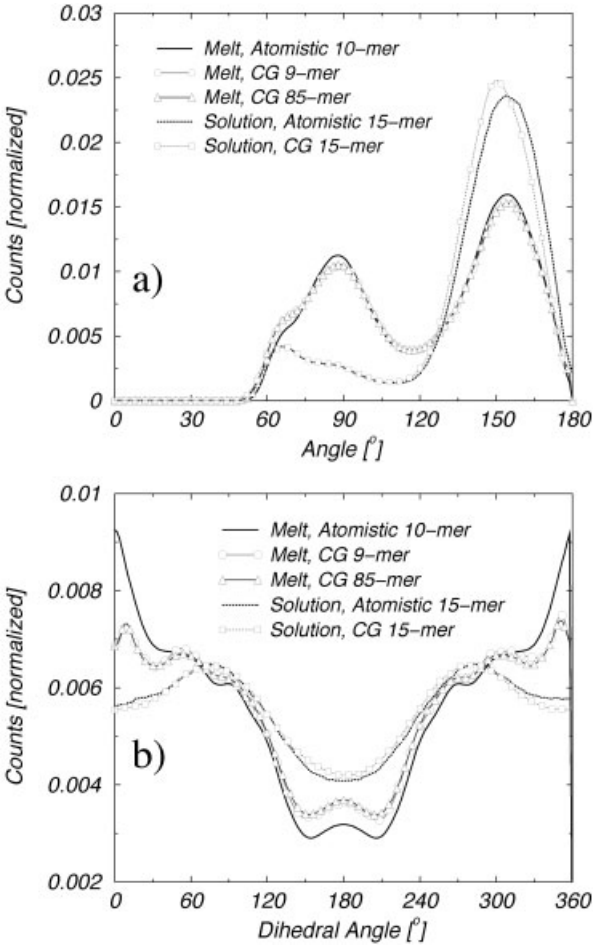

Figure 6. Histogram of (a) the angle between three successive coarse-graining (CG) points and (b) the dihedral for four successive CG points from atomistic and mesoscopic simulations of a polyisoprene. Melts as well as solutions are considered. In both cases (a) shows that the three peaks from the atomistic data (centered ≈70, 90, and 160°) are well reproduced by the CG simulations. In both graphs, the values are regularly off by not more than 10%, except for some areas in the case of the melt torsions (≈20%). No dependence on the chain length can be observed for the melts.

compared to the RDF-a ($r \approx 0.4$–0.8 nm) supports the statement that the chains are strongly curved, because such short distances are realized by intrachain contacts beyond second neighbor distances. The intermolecular RDF, as given in Figure 8 (solid line, "target RDF"), provides information on intermolecular contacts of the super-atoms. Major observations are the narrowness of the main peak at $r \approx 0.5$ nm and the lack of any further strong peaks.

The situation for the solution systems is slightly different. Figure 6 indicates that the chains are much more stretched out, especially because the fraction of bond angles around 160° dominates greatly over all other states. This picture is also visible in the intramolecular RDF, given in Figure 9. Clear peaks of first (≈0.47 nm), second (≈0.9 nm ≈ 2 × 0.47 nm), and third (≈1.3 nm ≈ 3 × 0.47 nm) neighbors corresponding to stretched-out states are sep-

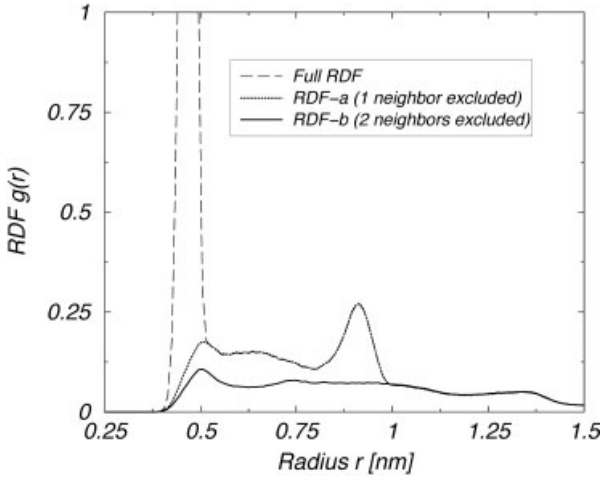

Figure 7. Intrachain radial distribution functions (RDFs) for superatoms as obtained from atomistic simulations of a polyisoprene melt (9-mers). RDF-a refers to an intrachain RDF for which we ignored the nearest neighbor chain particles. RDF-b denotes the intrachain RDF excluding the two next neighbors.

arated by low-populated areas in between. Most importantly, both the melt and the solution system deliver nicely peaked distribution functions with good statistical accuracy, providing a good starting point for the coarse graining.

Polyisoprene Melt Optimization

As target functions for the iterative Boltzmann inversion, both the intra- and intermolecular RDFs were chosen. The *physically* mean-

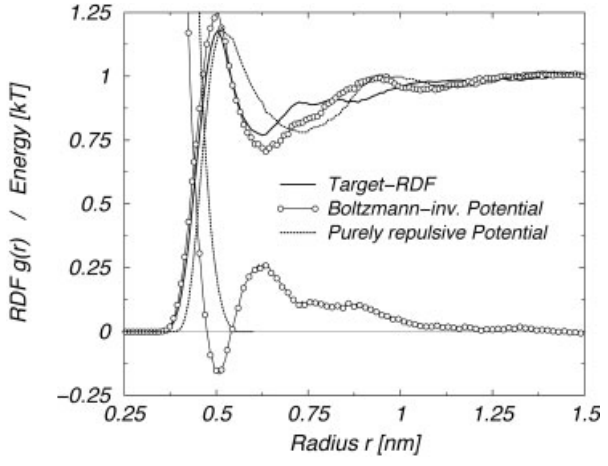

Figure 8. Interchain radial distribution functions (RDFs) for superatoms as obtained from atomistic simulations of a polyisoprene melt (9-mers) and for initial guesses of coarse-graining potentials: the RDFs that correspond to a simulation with the potential of mean force and a purely repulsive potential are shown. Compared with the target RDF from the atomistic simulations, they can both reproduce the rise of the main peak and the convergence against 1 for $r \gtrsim 1.25$ nm. However, the intermediate regime is badly mimicked.

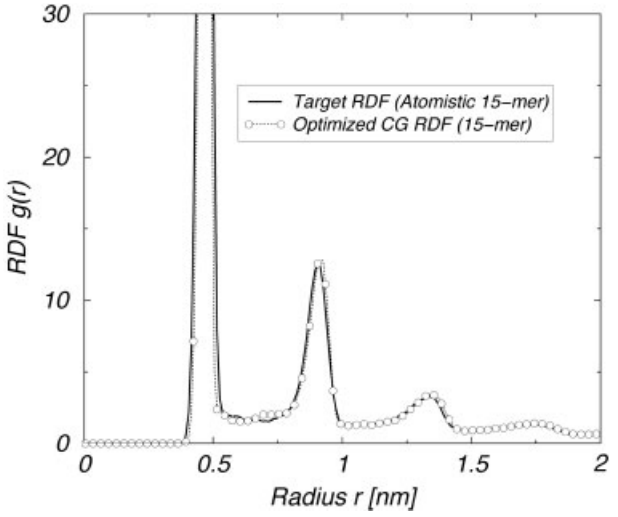

Figure 9. Intrachain radial distribution functions (RDFs) for superatoms as obtained from atomistic and mesoscopic simulations of a polyisoprene solution. In the case of the latter, the result of a coarse-graining optimization is shown. The coincidence of the curves is excellent.

ingful way to proceed has been described in full detail in a foregoing publication.[25] A viable course of action is to successively adjust the terms contributing to the total force field in the order of their relative strength:

$$V_{\text{stretch}} \rightarrow V_{\text{bend}} \rightarrow V_{\text{nonbonded}} \rightarrow V_{\text{dihedral}} \tag{3}$$

In contrast to the technique applied in ref. 25, the simplex algorithm, we now want to do the optimization with the iterative Boltzmann method.

Structure Optimization

The stretching potential V_{stretch} was considered first. The Gaussian shape of the distribution function turned out to be sufficiently mimicked by a Boltzmann-inverted potential without further optimization, as in the case of poly(acrylic acid) in solution.[25] So, this degree of freedom can be treated independently from all others. Next came the bending potential V_{bend}. As an initial guess (as for all other intramolecular force field terms), the Boltzmann-inverted distribution $P(\alpha)$ was applied, that is

$$V^0_{\text{bend}}(\alpha) = -k_B T \ln(P(\alpha)/\sin\alpha) \tag{4}$$

Then, we did a quick check of the distribution of the dihedral angle and found that the coincidence of the curves was already acceptable. Given the low importance of torsions, we therefore chose to apply a potential derived similarly to the one for the bending angle:

$$V^0_{\text{dihedral}}(\beta) = -k_B T \ln P(\beta) \tag{5}$$

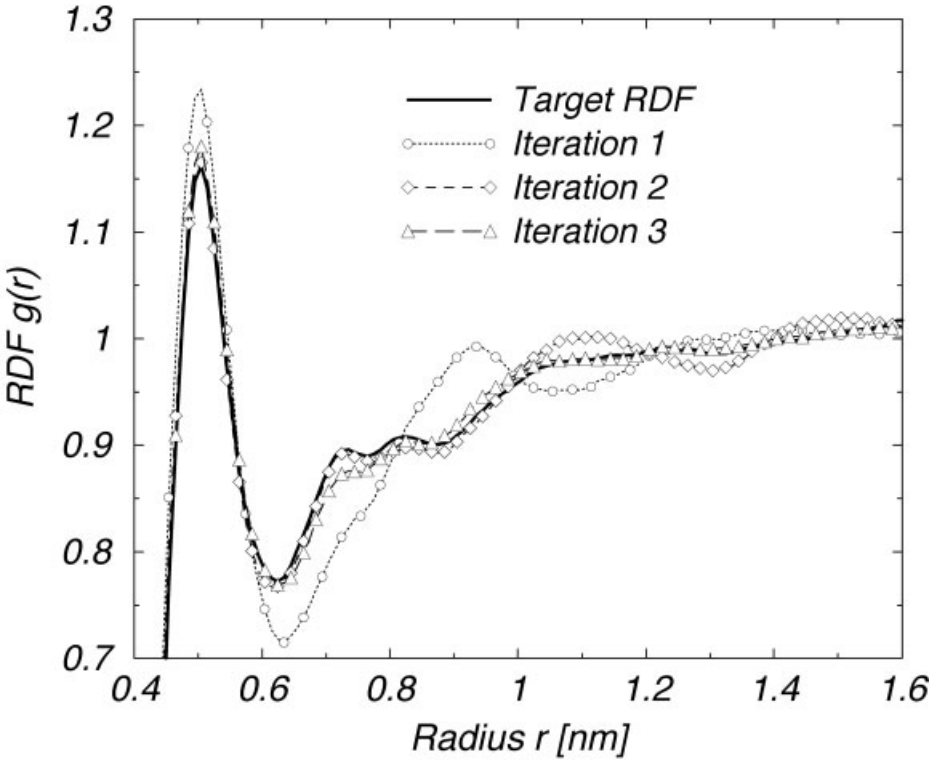

Figure 10. Optimization of the intermolecular RDF for a melt of polyisoprene 9-mers by way of the iterative Boltzmann method. The RDF of iteration 1 corresponds to the initial potential guess, the direct Boltzmann inversion of the intermolecular target RDF. The quality of the trial RDFs improves very fast. After the third iteration (shown), the trial RDFs match the target within line thickness (not shown any more).

Observe that the sinus-function originating from the Jacobi-transformation matrix when using spherical instead of Cartesian coordinates only appears for the half-sphere bending potential. A review of the dihedral distribution after optimizing the nonbonded part showed that it was not altered significantly. The result can be viewed in Figure 6. Similar conclusions were drawn by Tschöp et al. when deriving a CG force field for polycarbonates.[12]

Therefore, we turned to the most crucial step in the case of melts: optimizing the intermolecular interactions $V_{\text{nonbonded}}$. To get a feeling for the correct curvature of the intermolecular potential, we started with two different initial choices: first, a purely repulsive potential (WCA[34]), and second, the Boltzmann-inverted potential of the target RDF. The results are presented in Figure 8. Both reproduce the rise of the main peak and the convergence toward 1 for $r \gtrsim 1.25$ nm. The intermediate regime is badly reproduced. This was expected as higher order correlations are well captured with effective pair potentials. We chose to start the iteration with the Boltzmann inverse. The RDF converged quickly. The first three iterations are shown in Figure 10. The curve of iteration 1 is identical with the one shown in Figure 8. It is far off the target curve at most distances. Already, the second iteration $g_2(r)$, however, produces very good results up to a distance of around 1 nm. The third iteration $g_3(r)$ barely deviates from the target curve. Convergence can be measured quantitatively by evaluating the following merit function ($r_{\max} = 1.5$ nm):

$$f_{\text{target}} = \int w(r)(g(r) - g_j(r))^2 dr \tag{6}$$

As a weighting function, we apply $w(r) = \exp(-r/\sigma)$, in order to penalize more strongly deviations at small distances. The results are as follows:

```
#         f_target
Step 1    0.109621
Step 2    0.0107148
Step 3    0.0063149
Step 4    0.00223776
Step 5    0.00159995
Step 6    0.00144287
Step 7    0.00166992
Step 8    0.00128543
Step 9    0.00147876
```

Looking at the merit function we can see that the RDF converged after about five iterations. After that, the deviations must be regarded as pure noise within our statistical accuracy. One can also see that the potential solution remains stable. A close look at Figure 10 also reveals that the curves converge from short distances to large distances: areas that were mimicked very accurately

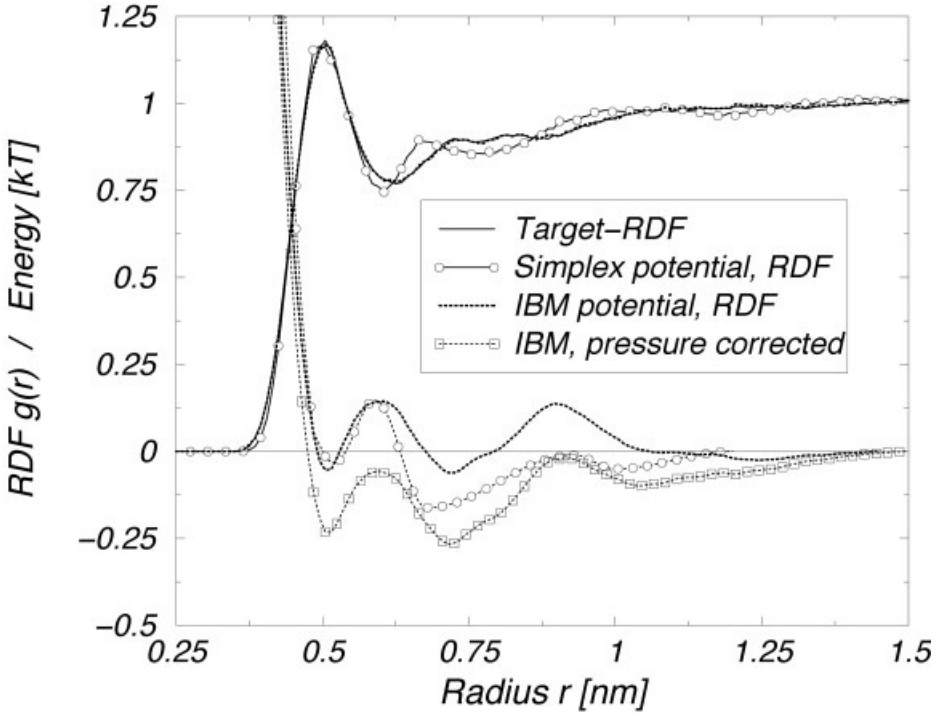

Figure 11. Converged RDFs for mesoscopic simulations of a polyisoprene melt. Using the simplex algorithm, the area $r \gtrsim 0.6$ nm could only qualitatively match the target RDF. In turn, the iterative Boltzmann-inversion leads to a trial RDF, which is identical to the target within line thickness. The last curve corresponds to the pressure-corrected result.

in an earlier iteration could be off in a subsequent one, if there were areas at shorter distances that did not match yet. This reflects the fact that changes in the potential are nonlocal: they might have an impact at larger distances, too. The final tabulated potential is shown in Figure 11. Note again that this potential is temperature and density dependent. Changes of more than a few percent must lead to a reparametrization of the whole force field. Some experience we had with this issue has already been described elsewhere.[36]

Simplex versus Iterative Boltzmann Optimization

Until recently, CG force field optimizations were also done by making use of the simplex algorithm in our group.[24,27] This procedure can be applied when manipulating parameters of analytical force field models. Typically, those contain several intra- and intermolecular terms, each of which consists of a specific set of parameters, say $p_1, \ldots, p_n$. For the iterative process, a single-valued merit function is needed to evaluate the actual set of parameters, and, hence, the corresponding potential trial functions:

$$f_{\text{target}} = f(\{p_k\}) \rightarrow \min! \tag{7}$$

Creating new sets of parameters in order to minimize the merit function can then be done by the simplex algorithm.[35] In the case of the optimization of structural properties, the merit function of eq. (6) was utilized.[25] In general, target values can come either from experimental data or from simulations on a different length scale. So far we have used thermodynamic state observables[24] as well as continuous functions as the RDF.[33,36]

In order to compare the capability of the simplex method to that of the iterative Boltzmann method, we attempted an independent optimization with the first one. We constructed the piecewise analytical trial potential for the simplex optimization as follows (ignoring an additional shift to $V = 0$ at r_{cut}):

$$V_{\text{nonbonded}}(r) = \begin{cases} \varepsilon_1\left(\left(\frac{\sigma_1}{r}\right)^8 - \left(\frac{\sigma_1}{r}\right)^6\right) + \varepsilon_2 & r < \sigma_1 \\ \varepsilon_2\left(\sin\frac{(\sigma_1 - r)\pi}{2(\sigma_2 - \sigma_1)}\right) + \varepsilon_2 & \sigma_1 \le r < \sigma_2 \\ \varepsilon_3\left(\cos\frac{(r - \sigma_2)\pi}{\sigma_3 - \sigma_2} - 1\right) & \sigma_2 \le r < \sigma_3 \\ \varepsilon_4\left(-\cos\frac{(r - \sigma_3)\pi}{\sigma_4 - \sigma_3} + 1\right) - 2\varepsilon_3 & \sigma_3 \le r < \sigma_4 \\ \varepsilon_5\left(\cos\frac{(r - \sigma_4)\pi}{\sigma_5 - \sigma_4} - 1\right) - 2(\varepsilon_3 - \varepsilon_4) & \sigma_4 \le r < \sigma_5 \\ \varepsilon_6\left(-\cos\frac{(r - \sigma_5)\pi}{\sigma_6 - \sigma_5} + 1\right) - 2(\varepsilon_3 - \varepsilon_4 + \varepsilon_5) & \sigma_5 \le r < r_{\text{cut}} \end{cases} \tag{8}$$

Figure 11 proves that this formula, however complicated and lengthy, was successfully adapted according to the needs imposed

Table 2. Nonbonded Interaction Force Field Parameters for the Coarse-Grained Model of a Polyisoprene Melt.

σ_1	ε_1	σ_2	ε_2	σ_3	ε_3	σ_4	ε_4	σ_5	ε_5	$\sigma_6 = r_{cut}$	ε_6
0.485	1.1	0.61	0.09	0.724	0.228	0.927	0.24	1.08	0.038	1.3	0.05

Force field parameters according to eq. (8), with σ in nm and ε in kT.

by the shape of the target RDF: it comprises the possibility to generate a third potential well. The idea to apply a third well (and its position) came from the visual inspection of the Boltzmann-inverted potential and its corresponding RDF (Fig. 8). The shape of the RDF up to $r \approx 0.625$ nm indicates that the first potential well is a bit too deep but still meaningful. In the subsequent area ($0.625 \text{ nm} < r < 0.85$ nm), the trial RDF lies lower than the target RDF. Therefore, we presumed a second potential well at around 0.7 nm would be needed to correct for this shortcoming. A similar observation was made for the area $r > 0.85$ nm and we tried a first guess well centered at $r = 1.1$ nm. These rough estimates were utilized to initialize a simplex optimization. The optimum, as shown in Figure 11, fulfilled the condition $f_{target} < 0.02$ and was reached after 150 iteration steps. More details of the optimization procedure are given in ref. 36. The final parameter set is listed in Table 2.

In summary, the simplex algorithm has also been proven to generate acceptable results. However, much experience, time, and physical intuition were needed to come to this final result. Its quality is not as good as the quality of the Boltzmann-inverted force field, although there are many similarities between them, observe Figure 11. Therefore, its applicability for structural problems seems to be inferior compared to the new inverted Boltzmann scheme. In retrospect it appears that the exponential weighting function used in the merit function does not punish the long range deviation in $g(r)$ enough. Thus, the difference in the merit function between the two optimization methods is small, although the inverted Boltzmann scheme produces visibly better results for second and third peaks in the correlation hole regime.

Pressure Correction

So far, we were just concerned with the structural optimization of the PI melt system. Our best potential (Fig. 11), however, has a positive pressure of $p^* = 1.92$ (given in reduced units[28]). This does not reflect the ambient conditions of the parent atomistic system.[37] This is a consequence of the simulation being run at constant volume and thermodynamic properties not being present in the merit function. As proof of the concept that pressure correction is possible, we tried to postoptimize the mesoscopic system without lowering the quality of RDF. The potential of a neutral system is always attractive at long range due to the dispersion interactions. Consequently, we chose an attractive linear tail function as a weak perturbation to the potential previously optimized without pressure correction:

$$\Delta V_{lin}(r) = A\left(1 - \frac{r}{r_{cutoff}}\right) \tag{9}$$

with $A = -0.1 k_B T$. The correction fulfills the following essential conditions: $\Delta V_{lin}(0) = A$ and $\Delta V_{lin}(r_{cutoff}) = 0$. The corrected potential was then taken as an initial guess of a reoptimization of the potential against the structure using the iterative Boltzmann method. After that, the pressure was re-evaluated and the procedure continued until $p^* < 0.005$. This condition was reached after 10 iteration cycles. The pressure-corrected potential is also shown in Figure 11. As suspected, the shape, and with it the forces, are very similar to the force field optimized without pressure corrections. The pressure correction manifests itself mostly in the potential region beyond $r > 1$ nm, which is not very important for the structural fit. It shifts the whole potentials downward, thus providing for the previously missing long-range attraction.

Polyisoprene in Cyclohexane: Solution Optimization and Comparison to the Melt

Our atomistic PI systems were highly diluted and only system S3 contained more than one PI 15-mer. Because statistical accuracy was not sufficient to analyze intermolecular RDFs, we chose to optimize intramolecular degrees of freedom only. However, one to four interactions and higher were considered in the same way as intermolecular contacts, and a purely repulsive potential was applied for all those interactions to complete the force field properly. The repulsive potential was based on information of the melt simulations: the repulsive part between $r = 0$ and the minimum was cut off at the minimum and shifted to zero. The optimization of the intramolecular part was done in the same order as described before (cf. the section Polyisoprene Melt Optimization). So, the stretching potential $V_{stretch}$ was again our starting point. As expected for this rigid degree of freedom, the distribution of the bond distances was close to a Gaussian shape and it could be mimicked with almost identical parameters as in the melt system. This means that it is almost independent of the concentration of the system, in contrast to all other degrees of freedom. For the bending potential V_{bend}, the Boltzmann-inverted distribution $P(\alpha)$ was taken as an initial guess, according to eq. (4). After five iterations, the agreement shown in Figure 6 was achieved. The coincidence of the main peak around 160° was still not perfect. This originated from the metric-tensor corrections (division by sin α), which magnify potential corrections too strongly. However, the result is still satisfactory. For the torsions, the curves were again acceptable without any optimization. This shows the value of meaningful initial guesses and the accuracy of Boltzmann-inverted potentials, at least for some degrees of freedom. Taking the intramolecular potentials together as force field, the resulting RDF matches the target RDF very well. Meaningful static properties could be derived, as published elsewhere.[30]

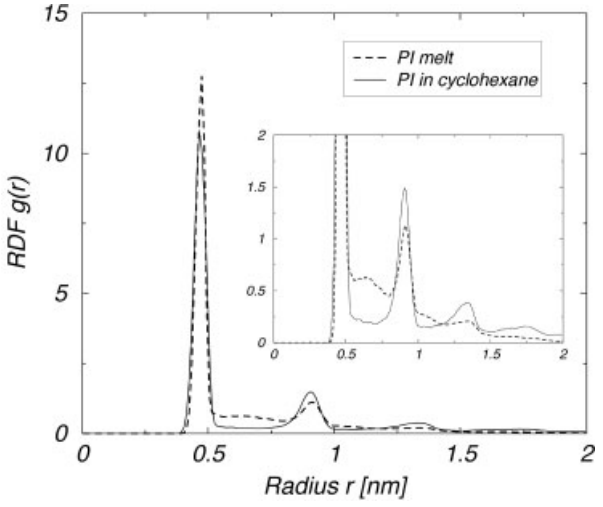

Figure 12. Comparison of intrachain radial distribution functions (RDFs) for super-atoms as obtained from mesoscopic simulations of a polyisoprene melt and dilute solution. The integrals under both curves have been normalized to 1 (with integral cutoff at $r = 2$ nm) in order to compare relative peak heights.

We are now also in the position to compare the intrachain RDFs of the mesoscopic simulations of a PI melt and a solution system. Figure 12 shows both curves with integrals normalized to 1 ($r_{cut} = 2$ nm) in order to compare relative peak heights. The fact that the intramolecular distribution functions are different is also reflected here: the peak positions are the same, but the relative intensity varies. In solution, the atomistic *trans* configuration is mesoscopically reflected by a high population of stretched-out states, due to good solvent conditions.

Discussion and Conclusions

In this contribution, we introduced an iterative method for potential inversion from distribution functions for polymer systems. However, this scheme could also be utilized for other chemical systems in which intramolecular connectivity has to be taken into account, such as low-molecular solvents or proteins. Basic tests on two monoatomic liquids (LJ and WCA) with known solutions showed that: in all cases the algorithm produced numerical potentials that led to RDFs undistinguishable from the target; the algorithm was robust and deviations between the iterative solution and the exact potential were minor; and the *a priori* unknown range of the potential is important. Note also that, taking numerical inaccuracies into account, the forces generated by different useful potentials are very similar to those observed in the corresponding graphs. As a conclusion, we would advocate starting with a range as small as possible and increasing it stepwise until deviations of the RDFs from their targets are satisfactory at all ranges.

The algorithm was applied to *trans*-1,4 polyisoprene oligomers in two different situations: melt and solution. Although the conformational differences between them inherited from the parent atomistic reference calculations still need to be understood more deeply, it is clear that iterative Boltzmann inversion can successfully coarse-grain both of them. The CG force fields turn out to be similar, but are clearly distinct from each other. For the melt system, it was also shown that the pressure could be postoptimized by adding a weak attractive perturbation potential without disturbing the short-range structure noticeably. This example illustrates nicely that, due to the neglect of (different) degrees of freedom during the CG procedure, the resulting CG potentials necessarily depend on the state of the polymer, here its environment: even the intramolecular parts of the potential differ in melt and solution.

Acknowledgments

We are indebted to Roland Faller for providing the atomistic force fields and part of the atomistic data of polyisoprene. Hendrik Meyer is deeply acknowledged for sharing his valuable ideas with us. We also want to thank Cameron Abrams for fruitful discussions.

References

1. van Gunsteren, W. F.; Berendsen, H. Angew Chem Int Ed Engl 1990, 29, 992.
2. de Gennes, P.-G. Scaling Concepts in Polymer Physics; Cornell University Press: Ithaca, 1979.
3. Doi, M.; Edwards, S. F. The Theory of Polymer Dynamics; Oxford University Press: Oxford, 1986.
4. Baschnagel, J.; Binder, K.; Doruker, P.; Gusev, A. A.; Hahn, O.; Kremer, K.; Mattice, W. L.; Müller-Plathe, F.; Murat, M.; Paul, W.; Santos, S.; Suter, U. W.; Tries, V. Adv Polym Sci 2000, 152, 41.
5. McCoy, J. D.; Curro, J. G. Macromolecules 1998, 31, 9362.
6. Bai, D.; Brandt, A. Multiscale Computation of Polymer Models. III. NATO Sci Ser 2001, 250.
7. Fukunaga, H.; Takimoto, J.; Doi, M. J Chem Phys 2002, 116, 8183.
8. Müller-Plathe, F. Chem Phys Chem 2002, 3, 754.
9. Murat, M.; Kremer, K. J Chem Phys 1998, 108, 4340.
10. Bolhuis, P. G.; Louis, A. A.; Hansen, J. P.; Meijer, E. J. J Chem Phys 2001, 114, 4296.
11. Louis, A. A. Philos T Roy Soc A 2001, 359, 939.
12. Tschöp, W.; Kremer, K.; Batoulis, J.; Bürger, T.; Hahn, O. Acta Polym 1998, 49, 61.
13. Hahn, O.; DelleSite, L.; Kremer, K. Macrom Th Sim 2001, 10, 288.
14. Akkermans, R. L. C.; Briels, W. J. J Chem Phys 2001, 114, 1020.
15. Schweizer, K. S.; Curro, J. G. J Chem Phys 1989, 91, 5059.
16. Weinhold, J. D.; Curro, J. G.; Habenschuss, A.; Londono, J. D. Macromolecules 1999, 32, 7276.
17. Pütz, M.; Curro, J. G.; Grest, G. S. J Chem Phys 2001, 114, 2847.
18. McGreevy, R. L.; Pusztai, L. Mol Simul 1988, 1, 359.
19. McGreevy, R. L. Nucl Instrum Meth A 1995, 354, 1.
20. Soper, A. K. Chem Phys 1996, 202, 295.
21. Evans, R. Mol Simul 1990, 4, 409.
22. Lyubartsev, A. P.; Laaksonen, A. Phys Rev E 1995, 52, 3730.
23. Lyubartsev, A. P.; Laaksonen, A. J Chem Phys 1999, 111, 11207.
24. Faller, R.; Schmitz, H.; Biermann, O.; Müller-Plathe, F. J Comput Chem 1999, 20, 1009.
25. Reith, D.; Meyer, H.; Müller-Plathe, F. Macromolecules 2001, 34, 2335.
26. Zwicker, J.; Lovett, R. J Chem Phys 1990, 93, 6752.

27. Reith, D.; Meyer, H.; Müller-Plathe, F. Comput Phys Commun 2002, 148, 299.
28. Allen, M. P.; Tildesley, D. J. Computer Simulation of Liquids; Oxford University Press: Oxford, 1987.
29. Faller, R.; Müller-Plathe, F.; Doxastakis, M.; Theodorou, D. N. Macromolecules 2001, 34, 1436.
30. Faller, R.; Reith, D. Macromolecules 2003, 36, 5406.
31. Faller, R. Ph.D. Thesis, Universität Mainz, 2000.
32. Grest, G. S.; Kremer, K. Phys Rev A 1986, 33, 3628.
33. Meyer, H.; Biermann, O.; Faller, R.; Reith, D.; Müller-Plathe, F. J Chem Phys 2000, 113, 6264.
34. Weeks, J. D.; Chandler, D.; Andersen, H. J Chem Phys 1971, 54, 5237.
35. Press, W. H.; Teukolsky, S. A.; Vetterling, W. T.; Flannery, B. P. Numerical Recipes in C: The Art of Scientific Computing; Cambridge University Press: New York, 1992; 2nd edition.
36. Reith, D. Ph.D. Thesis, Mainz University, Germany, 2001, http://archimed.uni-mainz.de/pub/2001/0074.
37. Faller, R.; Müller-Plathe, F. Chem Phys Chem 2001, 2, 180.